Available online at www.sciencedirect.com
ScienceDirect
Mendeleev Commun., 2016, **26**, 187–190
Mendeleev Communications

Hybrid materials based on core-shell polyorganosilsesquioxanes modified with iron nanoparticles

Alexander Yu. Vasil'kov,*[a] Dmitry A. Migulin,[b] Alexander V. Naumkin,[a] Olga A. Belyakova,[a] Yan V. Zubavichus,[c] Sergey S. Abramchuk,[a] Yuri V. Maksimov,[d] Sergey V. Novichikhin[d] and Aziz M. Muzafarov[a,b]

[a] *A. N. Nesmeyanov Institute of Organoelement Compounds, Russian Academy of Sciences, 119991 Moscow, Russian Federation. Fax: +7 499 135 5085; e-mail: alexandervasilkov@yandex.ru*
[b] *N. S. Enikolopov Institute of Synthetic Polymer Materials, Russian Academy of Sciences, 117393 Moscow, Russian Federation*
[c] *National Research Centre 'Kurchatov Institute', 123182 Moscow, Russian Federation*
[d] *N. N. Semenov Institute of Chemical Physics, Russian Academy of Sciences, 119991 Moscow, Russian Federation*

DOI: 10.1016/j.mencom.2016.04.002

A series of novel hybrid materials with the core-shell structure have been prepared by the immobilization of iron nanoparticles on branched polymethylsilsesquioxanes. The metal–vapor synthesis has been used for the generation of iron nanoparticles.

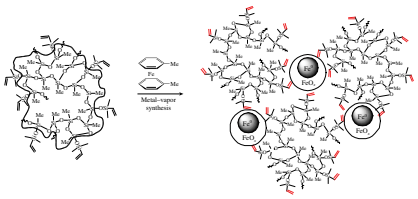

Branched organosilicon polymers are thermally stable and oxidation resistant. Furthermore, they manifest a high dielectric strength and miscibility towards diverse polymer materials.[1] Their based hybrid systems modified with metal nanoparticles are promising as advanced functional materials, such as catalysts, magnetics and antifriction compositions.

The metal–vapor synthesis (MVS) is a convenient and versatile route to the preparation of mono- and bimetallic nanoparticles and derived hybrid materials.[2]

The interaction of organosilicon systems with the single atoms or nanoparticles of noble metals (Pt or Au) generated *via* MVS affords new microheterogeneous metal complex catalysts and nanomaterials.[3,4] A high dielectric strength and bioinertness of organosilicon polymers combined with superparamagnetic properties of iron nanoparticles can be exploited for the design of efficient magnetic insulators, radar-absorbing coatings and biomedical materials.[5]

Here, we report the synthesis of novel iron-bearing organosilicon polymers based on a polymethylsilsesquioxane (PMSSO) nanogel obtained by polycondensation with the subsequent capping of hyperbranched PMSSO with functional tetramethyldivinyldisiloxane under active medium conditions.[6,†]

The *in situ* synthesis of the Fe/PMSSO hybrid material was accomplished by letting the organosilicon nanogel with the core–shell structure (with functional vinyl groups forming the outer shell of the macromolecule) in toluene to interact with thermally labile bis(toluene)iron ($T_{decomp} \approx -40$ °C), which has remained elusive so far for the traditional fine synthesis techniques but can readily be prepared in one step by the MVS method[2,5,7] (Scheme 1).

The reaction of organosilicon nanogels with the thermally labile Fe complex was accomplished in the so-called cryothermostating mode below the decomposition temperature of

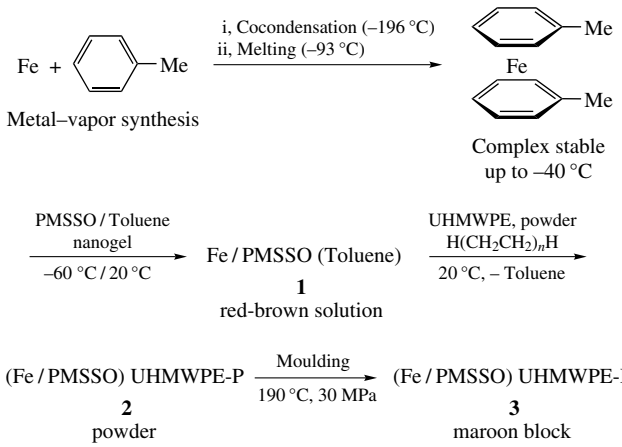

Scheme 1 Synthesis of hybrid materials based on organosilicon nanogels and ^{57}Fe nanoparticles.

the complex. The interaction of the iron complex with PMSSO nanogels in toluene affords a reddish-brown colloidal suspension of Fe/PMSSO **1**. We speculate that, in that reaction, a half-sandwich (η^6-toluene)iron complex additionally coordinates vinyl and oxygen-terminated moieties of the polymer. The affinity of (η^6-toluene)iron half-sandwich towards olefins[8] and the surfaces of inorganic oxide substrates[9] has been demonstrated earlier.

Presumably, a competing reaction proceeds along with the formation of **1**. Chemisorbed organometallic fragments and Fe nanoparticles react with the complex present in solution, which gives rise to core-shell Fe nanoparticles with the zero-valent core and outer shell of non-stoichiometric oxides upon temperature raise to room temperature.[2,5(*b*),10]

Figure 1 shows the TEM micrograph of Fe/PMSSO colloidal suspension in *n*-heptane. Silicone gel species (20–80 nm) encapsulated with Fe particles with a size of 2.3–4.7 nm can be clearly seen. The particles are uniformly distributed in the polymer matrix, which evidences the high stabilization ability of the nanogel.

† For procedures and characteristics of synthesized compounds, see Online Supplementary Materials.

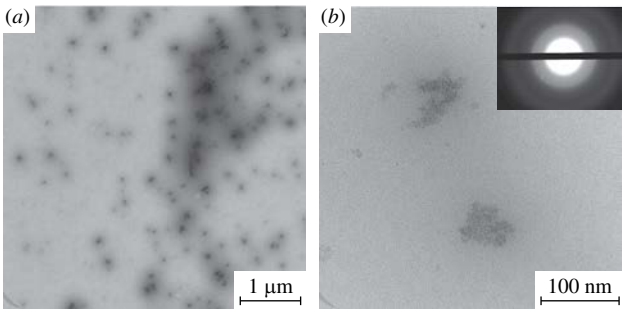

Figure 1 TEM micrographs of Fe/PMSSO colloidal suspension in *n*-heptane. Insert: selected-area electron diffraction (SAED) pattern.

On the surface of metal nanoparticles, a loose shell is observed most probably due to Fe–O bonds, which can be formed by the interaction of the metal surface with the functional groups of the polymer and by oxidation.

The typical selected-area electron diffraction (SAED) pattern is shown in Figure 1(*b*). The interplanar distances observed in the diffraction pattern are 2.03, 1.46, and 1.18 Å, which finely correspond to 2.0268, 1.4332 and 1.1702 Å typical of body-centered cubic lattice of α-Fe, respectively. Furthermore, a weak ring corresponding to an interplanar distance of 2.53 Å was resolved. It can be assigned to a spinel-type (Fe_3O_4 or γ-Fe_2O_3) lattice. Such a continuous broad ring may indicate the presence of significant amounts of iron oxide nanocrystals with a maximum size of 2–3 nm.

As it has been demonstrated earlier,[11] the hybrids of ultra-high molecular weight polyethylene (UHMWPE) and Fe nanoparticles can be used as efficient tribological modifiers. In particular, the surface of UHMWPE specimens was modified by Fe nanoparticles stabilized in the organosilicon nanogel (see Scheme 1). This can be used to tune the wear resistance and biocompatibility of such multifunctional materials.[12]

The treatment of UHMWPE with a toluene solution of **1** followed by solvent removal yields a uniform red-brown powder of (Fe/PMSSO) UHMWPE-P **2**. The metal content evaluated by XFA was 0.2 wt%. The powder of **2** can be compacted at 190 °C and 30 MPa to a bulk material of (Fe/PMSSO) UHMWPE-B **3**.

Mössbauer spectroscopy, which is an approved and highly informative technique for iron-containing species, was used to assess the composition, magnetic parameters, and size of nanoclusters in hybrid materials **1** and **3**. Figure 2 shows the Mössbauer spectra and their deconvolution into different Fe components for two composite samples Fe/PMSSO **1** and (Fe/PMSSO) UHMWPE-B **3** at different temperatures.

Room-temperature spectrum of **1** can be described by three major components, *viz.*, (i) a paramagnetic doublet from octahedrally coordinated Fe^{3+} in a high spin state with an isomer shift of δ = 0.35±0.03 mm s^{-1}, quadrupole splitting of Δ = = 0.95±0.03 mm s^{-1}, and a relative content of A = 0.41±0.05; (ii) a relaxation singlet characteristic of Fe^{3+} in superparamagnetic iron oxides[13] with a relative content of A = 0.36±0.05; (iii) magnetic hyperfine-split lines from zero-valent iron with δ = 0.04±0.03 mm s^{-1}, Δ = 0.02±0.03 mm s^{-1}, magnetic induction at a ^{57}Fe nucleus B_{in} = 32.5±0.5 T, and a relative content of A = 0.23±0.05.

The spectrum of **1** at 78 K can also be deconvolved into analogous three components: (i) a paramagnetic doublet with δ = 0.44±0.03 mm s^{-1}, Δ = 0.89±0.03 mm s^{-1}, and a relative content of A = 0.65±0.05; (ii) a relaxation component with δ = = 0.40±0.03 mm s^{-1} and a relative content of A = 0.25±0.05; (iii) magnetic HFS lines of the zero-valent metal with δ = = 0.23±0.03 mm s^{-1}, Δ = 0.02±0.03 mm s^{-1}, B_{in} = 35.0±0.5 T, and a relative content of A = 0.1±0.05. The significant increase

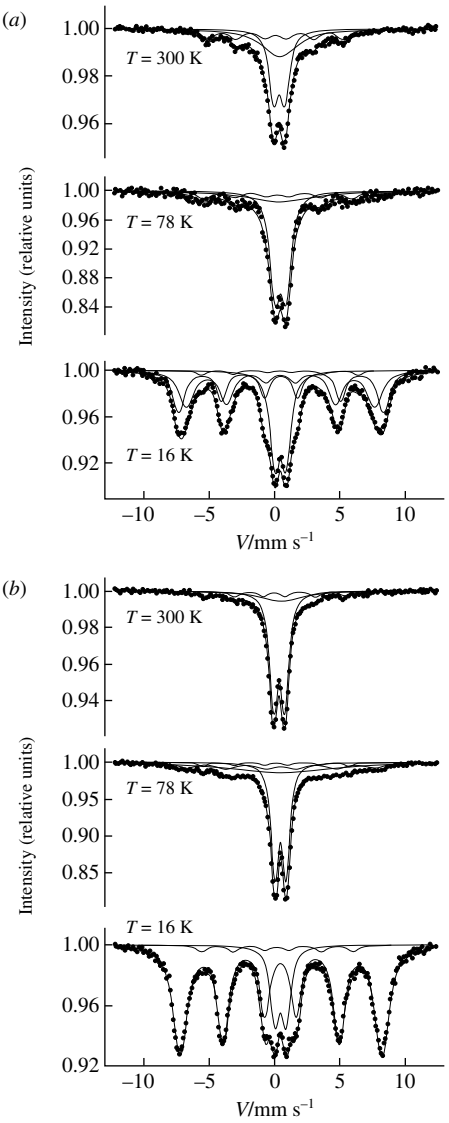

Figure 2 Mössbauer spectra for (*a*) Fe/PMSSO **1** and (*b*) (Fe/PMSSO) UHMWPE-B **3**.

in the fraction of the paramagnetic doublet at 78 K with respect to the room temperature spectrum can be rationalized as follows. Probably, at 300 K, iron atoms coordinated to the organosilicon nanogel possess a high mobility. The large amplitude of atomic vibrations reduces the probability of the Mössbauer effect. Within the Debye approximation, the Mössbauer factor is given by the expression $f = \exp(-k_\lambda^2 \langle x^2 \rangle)$, where λ is the wavelength, $k_\lambda = E_\lambda/\hbar c$ is the X-ray radiation wavenumber, and $\langle x^2 \rangle$ is the mean-square displacement of Fe atoms. The latter term $\langle x^2 \rangle$ is actually temperature dependent and can be expressed as $\langle x^2 \rangle/\lambda^2 = aT + bT^2$, where a and b are force constants of the respective chemical bonds in a solid phase.[14] At room temperature, the mean value of $\langle x^2 \rangle$ for Fe^{3+} atoms is large and the Mössbauer effect is strongly suppressed. A substantial increase in the fraction of the paramagnetic doublet at 78 K is due to the abrupt freezing of the atomic dynamics of polymer-coordinated iron ions.

A further temperature lowering to 16 K produces spectral changes highly specific to composites containing superparamagnetic iron oxide clusters. Indeed, more than a half of the intensity of the paramagnetic doublet component is transformed into a set of two hyperfine-split lines with magnetic inductions at a ^{57}Fe nucleus of $B_{in}(1)$ = 48.4±0.5 T and $B_{in}(2)$ = 44.4±0.5 T. These values and nearly zero quadrupole shifts for both lines are consistent with the spinel-type maghemite γ-Fe_2O_3 nanoparticles with a size of 3–5 nm.

The room temperature spectrum of **3**, as in the case of sample **1**, contains three main components: (i) a paramagnetic doublet of octahedrally coordinated Fe^{3+} ions in a high spin state with δ = = 0.35±0.03 mm s^{-1}, Δ = 0.87±0.03 mm s^{-1}, and a relative content of A = 0.70±0.05; (ii) a relaxation singlet from Fe^{3+} in a superparamagnetic state with δ = 0.49±0.03 mm s^{-1} and a relative content of A = 0.19±0.05; (iii) HFS lines from zero-valent iron with δ = –0.01±0.03 mm s^{-1}, Δ = 0.00±0.03 mm s^{-1}, magnetic induction at a ^{57}Fe nucleus of B_{in} = 32.9±0.5 T and a relative content of A = 0.11±0.05.

Nevertheless, in contrast to sample **1**, the spectrum of **3** at 78 K demonstrates a remarkable decrease in the fraction of the paramagnetic doublet down to 0.44 with a simultaneous increase in the relative intensity of the relaxation component up to ~0.33 and appearance of HFS lines from magnetic maghemite clusters with B_{in} = 45.2±0.5 T and a relative content of A = 0.18±0.05. The component of HFS lines of metallic iron manifests only minor changes. A decrease in the temperature to 16 K leads to a further drop in the paramagnetic doublet intensity down to a fraction of A = 0.1±0.05. The spectrum at that is dominated by a very intense magnetic HFS lines with δ = 0.48±0.03 mm s^{-1}, Δ = 0.00±0.03 mm s^{-1}, B_{in} = 47.8±0.5 T, and a fraction of A = 0.83±0.05. Low-intensity lines of metallic iron with δ = = 0.20±0.03 mm s^{-1}, Δ = 0.00±0.03 mm s^{-1}, B_{in} = 36.0±0.5 T, a fraction of A = 0.06 remain in the spectrum.

Such a complicated behavior of temperature-induced spectral changes can be rationalized as follows. Two dynamic effects compete in samples **1** and **3**: one is associated with the real thermal motion of Fe atoms and another one, with the dynamics of their spins. The former effect prevailed in **1** at 300 K: a large portion of Fe^{3+} ions located at the surface of maghemite nanoparticles (2–3 nm) and coordinated to oxygen-containing groups of the organosilicon nanogel are characterized by very large mean-square displacements that suppress the Mössbauer effect. Essentially, the polymer nanogel matrix behaves as a quasi-liquid that becomes more solid-like upon freezing to 78 K and further down to 16 K. Moreover, the low-temperature spectra are dominantly formed by superparamagnetic iron oxide clusters.

The chemical composition and electronic states of functional groups at the surface of the hybrid materials were elucidated with the use of XPS. The Fe 2*p* core-level spectrum for **3**, as shown in Figure 3, is characterized by a poor signal-to-noise ratio due to the very low concentration of iron at the material surface. Nevertheless, the spectrum can be reliably described by two Gaussian profiles of a 2p spin-orbital doublet with binding energies of 711.4 and 725.4 eV and respective FWHMs of 3.6 and 5.0 eV. The combination of spin-orbit splitting of 13.0 eV and binding energies can be reliably assigned to nanosized γ-Fe_2O_3 or Fe_3O_4 according to published data.[15]

The O 1*s* core-level spectrum reveals no FeO_x component, which means a low concentration of iron and its oxides within the near-surface regions. This may indicate that iron oxide particles are effectively coated by a polymer shell. Unfortunately, no information on the chemical nature of interactions between Fe nanoparticles and organosilicon nanogels can be derived from current XPS data. Nevertheless, the XPS data are consistent with the above interpretation of Mössbauer data.

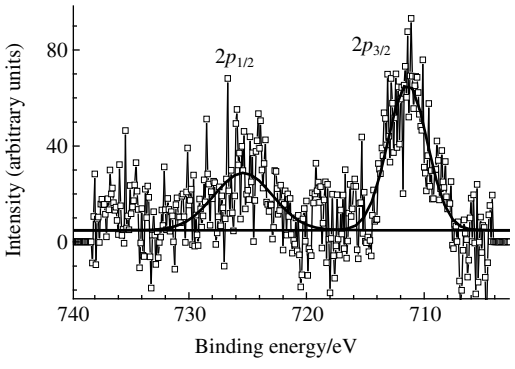

Figure 3 Fe 2*p* core-level spectrum for (Fe/PMSSO) UHMWPE-B **3**.

The insight into the chemical state of iron atoms in the hybrid materials was obtained by XANES spectroscopy. The experimental Fe K-edge XANES spectrum of **3** is compared to the spectra of reference compounds, *i.e.*, Fe foil and γ-Fe_2O_3 maghemite in Figure 4(*a*). The energy position and general shape of the near-edge fine structure taking into account the region of the pre-edge resonance in the XANES spectrum of **3** are quite similar to those of maghemite except for a more smeared character. This means that the chemical state of iron in hybrid material **3** is similar to that in maghemite, *i.e.*, iron occurs dominantly in the oxidation state +3, and the iron cations are surrounded by oxygen atoms in octahedral and tetrahedral configurations. The fraction of Fe in other oxidation states, such as +2 and 0, is small. We attempted to deconvolve the experimental XANES spectrum into a linear combination of reference spectra including Fe foil and maghemite, but this procedure consistently yielded a negligible fraction of Fe^0.

However, the Fourier transform of Fe K-edge EXAFS spectra shown in Figure 4(*b*) reveals important differences between **3** and maghemite, especially prominent in the region of the second coordination sphere, which challenges the suggestion on complete equivalency of the local structure of Fe-containing clusters in the organosilicon matrix to iron oxide nanoparticles. The first coordination sphere is well fitted with a single Fe–O contribution at an interatomic distance of 1.95–1.97 Å and an effective coordination number of around 4. The introduction of additional contributions of light atoms at distances of 2.1–2.2 Å (for instance, anticipated for coordinated vinyl groups) does not improve the fit quality. An adequate description of the second coordination sphere requires a superposition of several nonequivalent components. The best fit was obtained for a combination of three contributions: direct Fe–Fe metal–metal bonds (as in the bulk metal phase), non-bonded Fe···Fe contacts *via* the oxygen bridges (present in the ordered iron oxide phases), and non-bonded Fe···Si contacts (*via* the oxygen bridges). The fit quality factor R_f gets much worse if any of these contributions is not included into the structural model (a representative set of fitted models is given in Table 1). This is especially true for the metallic bonds Fe–Fe contribution, despite the fact that the best-fit coordination number for this coordination sphere is quite small. Therefore, based on EXAFS local structure information, we can conclude that the iron atoms in the hybrid materials most probably form oxide nanoparticles closely related structurally to maghemite. A small fraction of iron (about 5% is in accordance with an estimate from

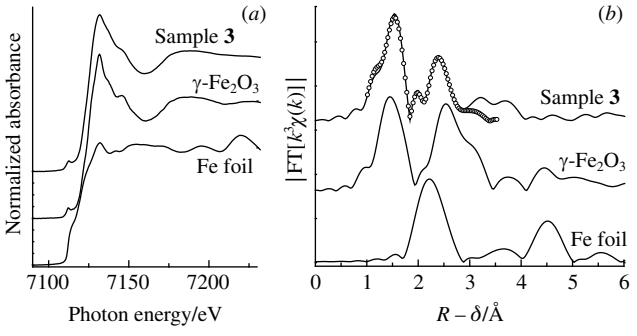

Figure 4 (*a*) Fe K-edge XANES spectra of hybrid material **3** and reference compounds and (*b*) Fourier transform of Fe K-edge EXAFS spectra of hybrid material **3** and reference compounds (uncorrected for the phase shift δ). For sample **3**, the best-fit theoretical curve (corresponding to structural model 1 from Table 1) is shown with open circles.

Table 1 Parameters of local environment of Fe atoms in **3** from a quantitative analysis of EXAFS data for selected structural models: coordination numbers (CN) and interatomic distances (*R*). Nominal accuracy of the fitting procedure is ±10% for CN and ±0.01–0.02 Å for *R*.

Model no.	R_f	Scattering path	CN	*R*/Å
1	0.008	Fe–O	4.2	1.97
		Fe–Fe	0.3	2.60
		Fe···Fe	4.0	2.98
		Fe···Si	2.4	3.34
2	0.014	Fe–O	5.0	1.97
		Fe–Fe	0.3	2.60
		Fe···Fe	8.9	3.02
3	0.016	Fe–O	3.7	1.95
		Fe–Fe	0.4	2.59
		Fe···Si	5.0	3.24

Mössbauer spectroscopy) form Fe^0 metal clusters. The iron oxide nanoparticles are stabilized by interaction with terminal oxygen-containing groups of the polyorganosiloxane matrix.

Thus, for the first time, the systems based on superparamagnetic Fe particles stabilized in the polymethylsilsesquioxanes nanogel matrix, Fe/PMSSO, have been prepared. It was found that the silicone nanogels composed of Fe^0 and γ-Fe_2O_3 species stabilize metal particles with a size of 2–3 nm. It was shown that the Fe/PMSSO system is an effective modifier for the formation of metal-containing hybrid materials based on ultra-high molecular weight polyethylene.

The modification of Fe nanoparticles with a silicone polymer leads to the formation of a nanocomposite containing particles with the Fe^0–FeO_x core-shell structure. The formation of the nanocomposite probably proceeds in two steps. The first occurs *in situ* by reacting bis(toluene)iron and the polymer to form **1**. The second step of metal nanostructure formation occurs in air during the preparation of hybrid material **3** with UHMWPE. Mössbauer spectroscopy measurements at 300 K showed Fe^0 contents of 23 and 11% in nanocomposites **1** and **3**, respectively. It can be assumed that the oxidation of iron during the first step is due to its interaction with the organosilicon nanogels, while the further decrease in the content of zero-valent metal by 12% is caused by the air-permeability of the resultant hybrid material.

This work was supported in part by the Russian Foundation for Basic Research (grant no. 14-03-01074) and the Russian Science Foundation (grant no. 14-23-00231).

Online Supplementary Materials

Supplementary data associated with this article can be found in the online version at doi:10.1016/j.mencom.2016.04.002.

References

1 (*a*) L. J. Mathias and T. W. Carothers, in *Advances in Dendritic Macromolecules*, ed. G. R. Newkome, JAI Press, Greenwich, 1995, p. 101; (*b*) H. Frey and C. Schlenk, in *Topics in Current Chemistry*, ed. F. Vogtle, Springer, Berlin, 2000, vol. 210, pp. 69–129; (*c*) J. Manfred, E. Rebrov, V. Kazakova, A. Muzafarov, W. Goedel and M. Moller, *Macromol. Chem. Phys*., 2003, **204**, 1014.

2 (*a*) J. J. Schneider, N. Czap, J. Hagen, J. Engstler, J. Ensling, P. Gütlich, U. Reinoehl, H. Bertagnolli, F. Luis, L. J. de Jongh, M. Wark, G. Grubert, G. L. Hornyak and R. Zanoni, *Chem. Eur. J.*, 2000, **6**, 4305; (*b*) K. A. Easom, K. J. Klabunde, C. M. Sorensen and G. C. Hadjipanayis, *Polyhedron*, 1994, **13**, 1197; (*c*) V. G. Nenajdenko, A. Yu. Vasil'kov, A. A. Goldberg, V. M. Muzalevskiy, A. V. Naumkin, V. L. Podshibikhin, A. V. Shastin and E. S. Balenkova, *Mendeleev Commun.*, 2010, **20**, 200; (*d*) A. Yu. Vasilkov, A. V. Naumkin, I. O. Volkov, V. L. Podshibikhin, G. V. Lisichkin and A. R. Khokhlov, *Surf. Interface Anal.*, 2010, **42**, 559; (*e*) A. Yu. Vasil'kov, M. S. Rubina, A. A. Gallyamova, A. V. Naumkin, M. I. Buzin and G. P. Murav'eva, *Mendeleev Commun*., 2015, **25**, 358.

3 (*a*) G. Uccello-Barretta, F. Balzano, C. Evangelisti, P. Raffa, A. Mandoli, S. Nazzi and G. Vitulli, *J. Organomet. Chem.*, 2008, **693**, 1276; (*b*) G. Uccello-Barretta, C. Evangelisti, P. Raffa, F. Balzano, S. Nazzi, G. Martra, G. Vitulli and P. Salvadori, *J. Organomet. Chem.*, 2009, **694**, 1813.

4 B. L. V. Prasad, S. I. Stoeva, C. M. Sorensen, V. Zaikovski and K. J. Klabunde, *J. Am. Chem. Soc.*, 2003, **125**, 10488.

5 (*a*) A. Yu. Vasil'kov, B. A. Zachernyuk, Z. N. Karpikov, I. O. Volkov, Ya. V. Zubavichus, A. A. Veligzhanin, A. A. Chernyshov, M. I. Buzin, L. N. Nikitin and V. I. Nedel'kin, *Russ. J. Appl. Chem.*, 2007, **80**, 2136 (*Zh. Prikl. Khim.*, 2007, **80**, 2058); (*b*) A. V. Naumkin and A. Yu. Vasil'kov, *Russ. Chem. Bull., Int. Ed*., 2013, **62**, 2559 (*Izv. Akad. Nauk, Ser. Khim.*, 2013, 2559); (*c*) S. Laurent, D. Forge, M. Port, A. Roch, C. Robic, L. Vander Elst and R. N. Muller, *Chem. Rev.*, 2008, **108**, 2064.

6 (*a*) E. V. Egorova, N. G. Vasilenko, N. V. Demchenko, E. A. Tatarinova and A. M. Muzafarov, *Dokl. Chem. (Engl. Transl.)*, 2009, **424**, 15 (*Dokl. Akad. Nauk*, 2009, **424**, 200); (*b*) D. Migulin, E. Tatarinova, I. Meshkov, G. Cherkaev, N. Vasilenko, M. Buzin and A. Muzafarov, *Polym. Int.*, 2016, **65**, 72; (*c*) E. A. Rebrov and A. M. Muzafarov, *Heteroat. Chem.*, 2006, **17**, 514.

7 (*a*) V. S. Asirvatham, Z. Yao and K. J. Klabunde, *J. Am. Chem. Soc.*, 1994, **116**, 5493; (*b*) J. J. Schneider, U. Specht, R. Goddard, C. Krüger, J. Ensing und P. Gütlich, *Chem. Ber*., 1995, **128**, 941; (*c*) Z. Yao, K. J. Klabunde and A. S. Asirvatham, *Inorg. Chem*., 1995, **34**, 5289; (*d*) Z. Yao, K. J. Klabunde and A. C. Hupton, *Inorg. Chim. Acta*, 1997, **259**, 119; (*e*) Z. Yao and K. J. Klabunde, *Inorg. Chem*., 1997, **36**, 2119; (*f*) J. J. Schneider, J. Hagen, N. Czap, C. Krüger, S. A. Mason, R. Bau, J. Ensling, P. Gütlich and B. Wrackmeyer, *Chem. Eur. J*., 2000, **6**, 625.

8 J. J. Schneider, J. Hagen, D. Bläser and R. Boese, *J. Am. Chem. Soc.*, 1999, **121**, 1409.

9 S. J. Woo, J. Godber and G. A. Ozin, *J. Mol. Catal.*, 1989, **52**, 241.

10 A. Yu. Vasil'kov, I. P. Suzdalev, Yu. V. Maksimov, L. N. Nikitin, A. V. Naumkin, S. S. Abramchuk, E. M. Tolstopyatov and P. N. Grakovich, *Russ. J. Phys. Chem. A*, 2013, **87**, 985 (*Zh. Fiz. Khim*., 2013, **87**, 1001).

11 A. P. Krasnov, V. A. Sergeev, L. B. Makina, P. V. Pribytkov, A. Yu. Vasil'kov, S. Yu. Panov and V. V. Anokhin, *Phys. Chem. Mech. Surf*., 1995, **10**, 1312.

12 A. P. Krasnov, E. E. Said-Galiev, A. Yu. Vasil'kov, A. Yu. Nikolaev, V. L. Podshibikhin, O. V. Afonicheva, V. A. Mit', A. R. Khokhlov, N. S. Gavryushenko, V. G. Bulgakov and S. P. Mironov, *RF Patent, 2 354 668 C1*, 2009.

13 I. P. Suzdalev, Yu. V. Maksimov, V. K. Imshennik, S. V. Novichikhin, V. V. Matveev, A. S. Plachinda and C. R. Lin, *Nanotechnol. Russia*, 2012, **7**, 345 (*Rossiiskie Nanotekhnologii*, 2012, **7**, 16).

14 (*a*) *Chemical Application of Mössbauer Spectroscopy*, eds. V. I. Goldanskii and H. Herber, Academic Press, New York, 1968; (*b*) K. A. Easom, K. J. Klabunde, C. M. Sorensen and G. C. Hadjipanayis, *Polyhedron*, 1994, **13**, 1197.

15 (*a*) S. J. Roosendaal, B. van Asselen, J. W. Elsenaar, A. M. Vredenberg and F. H. P. M. Habraken, *Surf. Sci*., 1999, **442**, 329; (*b*) T. Yamashita and P. Hayes, *Appl. Surf. Sci*., 2008, **254**, 2441; (*c*) B. J. Tan, K. J. Klabunde and P. M. A. Sherwood, *Chem. Mater*., 1990, **2**, 186; (*d*) D. T. Harvey and R. W. Linton, *Anal. Chem*., 1981, **53**, 1684.

Received: 26th November 2015; Com. 15/4782